Schottky-Contact Formation between Metal Electrodes and Molecularly Doped Disordered Organic Semiconductors

Lishuai Yu,[1] Qingqing Zhang,[1] Zhengpin Bian,[1] Guangzheng Zuo ,[5] Harm van Eersel,[4] Peter A. Bobbert,[2] Reinder Coehoorn ,[1,2] Feilong Liu ,[1,*] and Guofu Zhou[1,3,†]

[1]*Guangdong Provincial Key Laboratory of Optical Information Materials and Technology & Institute of Electronic Paper Displays, South China Academy of Advanced Optoelectronics, South China Normal University, Guangzhou 510006, People's Republic of China*

[2]*Department of Applied Physics and Institute for Complex Molecular Systems, Eindhoven University of Technology, Eindhoven University of Technology, P.O. Box 513, Eindhoven 5600 MB, Netherlands*

[3]*Shenzhen Guohua Optoelectronics Tech. Co. Ltd., Shenzhen 518110, People's Republic of China*

[4]*Simbeyond B.V., Het Eeuwsel 57, Eindhoven 5612 AS, Netherlands*

[5]*School of Information Science and Technology, Fudan University, Shanghai 200438, People's Republic of China*

We study using three-dimensional kinetic Monte Carlo (KMC) simulations to what extent the formation of Schottky contacts between a metal electrode and a molecularly doped disordered organic semiconductor can be understood from the theory for crystalline inorganic semiconductors, adapted to include the effects of the localized nature of the states in which the charge carriers reside and the hopping transport in between these states. The thickness of the Schottky-contact depletion region is found to be significantly smaller than as expected when the energetical disorder is neglected. The presence of energetic disorder is also found to influence the voltage dependence of the width of the depletion regions near the contacts of single-layer double-Schottky-contact devices. The voltage drop over the two depletion regions and the remaining charge-neutral bulk layer is shown to be described successfully by a semianalytical model, based on an accurately parameterized bulk mobility function of the dopant concentration, energetic disorder, and the electric field. We furthermore find that the mobility in the depletion regions is drastically reduced. As a result, the depletion-region formation process can be ultraslow, with a characteristic time scale ranging from microseconds to beyond milliseconds.

I. INTRODUCTION

Organic light-emitting diodes (OLEDs) have become one of the key technologies in display applications such as mobile phones and wearable devices. Under an external bias voltage, electrons and holes are injected from electrodes, move through the device, and recombine into excitons that decay radiatively under the emission of a photon. The onset voltage is often reduced by making use of thin molecularly doped "injection layers" in direct contact with the metal electrodes, which facilitate efficient charge injection [1–7]. In a hole injection layer, the lowest unoccupied molecular orbital (LUMO) energy of the dopant molecules is lower than or comparable with the highest occupied molecular orbital (HOMO) energy of the host material. The dopant molecules can then spontaneously

accept an electron from a nearby host molecule, leading to a relatively large concentration of "free" holes in the host material. An analogous process occurs in electron injection layers, within which the HOMO energy of the dopants is higher than or comparable with the LUMO energy of the host.

Currently, the models in the literature describing the doping physics for disordered organic semiconductors focus mostly on charge-neutral systems [8–14]. Experimentally, it has been shown that the charge-carrier mobility in *homogeneous* disordered organic semiconductors depends on the temperature, the electric field, and the charge-carrier concentration [15–17]. It has also been shown that the electrical conductivity of *molecularly doped* disordered organic semiconductors depends nonlinearly on doping concentration [18–20]. Based on these results, three-dimensional (3D) discrete lattice models with a Gaussian density of states (DOS) and three-dimensional kinetic Monte Carlo (3D-KMC) simulation techniques of localized charge-carrier dynamics were

---

*feilongliu@m.scnu.edu.cn
†guofu.zhou@m.scnu.edu.cn

developed [21–26]. These models can successfully explain measured electrical characteristics of OLEDs and have recently been applied to study the physics of molecularly doped systems [9–14]. From these simulation studies, it was found that a released charge carrier is not completely free to move, but stays at a nearby host molecule. Such a Coulombically bound pair of a charge carrier and an ionized dopant is called an "integer charge-transfer complex" (ICTC). The binding energy of the ICTCs and the energetic disorder determine together the precise shape of the nonlinear relationship between the electrical conductivity and the doping concentration [9].

When a doped inorganic crystalline semiconductor is in contact with a metallic electrode, the metal and semiconductor Fermi levels align, leading to band bending and the formation of a charge-carrier depletion region. The width of the depletion region is well understood from the Schottky-contact theory [27]. Inorganic crystalline semiconductors are characterized by covalent interatomic bonds and high-mobility band transport due to delocalized electrons or holes. It is not evident to what extent the conventional Schottky-contact theory can also be applied to molecularly doped disordered organic semiconductors, with weak van der Waals-type intermolecular interactions and a relatively low mobility due to hopping transport of localized charge carriers. In this work, we study systematically the formation and width of the charge-carrier depletion region of such systems under equilibrium conditions, when applying a constant bias voltage, and under dynamical conditions. We investigate how the depletion region depends on the material-specific properties such as the energetic disorder and the relative dielectric permittivity. The analysis is restricted to materials with all ionized dopants. Using 3D-KMC simulations, we show to what extent the barrier formation process and the current-voltage characteristics of devices can be described by adapted forms of the conventional inorganic semiconductor Schottky-contact model.

The paper is organized as follows. In Sec. II, we study metal-organic semiconductor Schottky contacts under equilibrium conditions, and show using 3D-KMC simulations that the width of the depletion region can be understood well from a semianalytical model. The charge-carrier mobility in charge-neutral and charged molecularly doped materials is studied using 3D-KMC simulations in Sec. III. The resulting dopant density, electric field, and charge-carrier density-dependent mobility functions are used in Sec. IV in a semianalytical model that is shown to provide a good description of the widths of the two depletion zones in single-layer double-Schottky-contact devices at a finite dc bias voltage, and of the voltage drops across these depletion zones. In Sec. V the transient response of a Schottky contact to a voltage change is discussed. It is found that the contact formation dynamics can be ultra-slow as a result of a very small charge-carrier mobility in

the depletion layers. Section VI contains a summary and outlook.

II. DEPLETION REGION WIDTH—EQUILIBRIUM

A. Semianalytical models

We focus first on the depletion region that is formed under equilibrium conditions. Throughout this paper, results are given for the case of *n*-doped organic semiconductors within which the ionization energy of the dopants is much smaller than the electron affinity, $E_{\mathrm{EA},h}$, of the host material, so that all dopants are ionized (full ionization). For inorganic crystalline semiconductors, the electron affinity is equal to the difference between the vacuum energy and the energy of the bottom of the conduction band. For disordered organic semiconductors, we assume that the distribution of electron affinities has a Gaussian shape with a width (standard deviation) σ. Figure 1(a) gives a schematic view of the energy-level diagram, indicating the disorder-averaged lowest unoccupied molecular energy of the host material, $E_{\mathrm{LUMO},h}$, and the highest occupied molecular orbital energy of the guest (dopant) molecules, $E_{\mathrm{HOMO},g}$. Figure 1(b) shows the energy-level structure of a single layer of such a material in between two identical electrodes at a voltage $V = 0$. We use the nomenclature that is conventionally used [27]. The nominal electron injection barrier, $e\phi_{Bn}$, is defined as $e\phi_{Bn} = e\Phi_M - E_{\mathrm{EA},h}$, with $e\Phi_M$ the work function of the metal
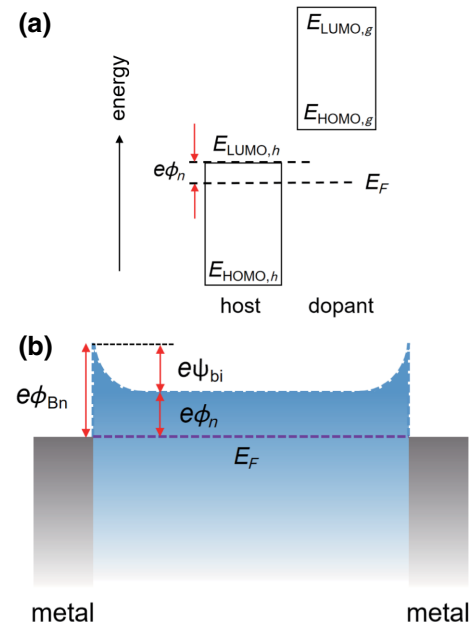
FIG. 1. (a) Schematic energy-level diagram for an *n*-type molecularly doped organic semiconductor. The disorder-induced energetic distribution of the states is not shown. (b) Energy diagram of such a semiconductor sandwiched in between two identical electrodes, forming two Schottky junctions at equilibrium ($V = 0$).

electrode and e the elementary charge. The formation of a depletion region gives rise to band bending that is characterized by a built-in voltage ψ_{bi}, and the energy difference between the maximum of the Gaussian LUMO DOS and the Fermi energy is termed $e\phi_n$.

Within the Schottky-contact model, the charge density in a depletion region of width W_D is assumed to be uniform and approximately equal to eN_D, with N_D the dopant volumetric density, whereas outside that region the semiconductor is assumed to be charge neutral. Simple electrostatics leads then to a quadratic spatial variation of the electrostatic potential in the depletion region and to a voltage (V) dependent depletion region width [27]

$$W_D = \sqrt{\frac{2\varepsilon_0\varepsilon_r}{eN_D}\left(\phi_{Bn} - \phi_n(N_D) - V - \frac{k_BT}{e}\right)}, \quad (1)$$

with ε_0 the vacuum permittivity, ε_r the relative dielectric constant, T the temperature and k_B the Boltzmann constant. The term k_BT/e arises from a thermally induced reduction of the positive space charge in the depletion region near the transition to the charge-neutral region [27].

The only parameter in Eq. (1) that depends on the material-specific conduction electron or LUMO DOS is the dopant-density-dependent energy $\phi_n(N_D)$. We first neglect the distortion of the DOS due to the positively charged ionized dopants. For energetically disordered systems with a Gaussian DOS

$$g_1(E) = \frac{1}{\sqrt{2\pi}\sigma}\exp\left(-\frac{E^2}{2\sigma^2}\right) \quad (2)$$

the energy $e\phi_{n,dis}$ can then be obtained numerically from Fermi-Dirac statistics using

$$N_D = \int_{-\infty}^{+\infty}\frac{g_1(E)N_0}{1 + \exp\left((E + e\phi_n)/k_BT\right)}dE, \quad (3)$$

where N_0 is the molecular density and N_D the electron density after full ionization of the dopants. As a reference, we consider systems with a δ-function DOS. The value of $e\phi_n$ is then given by

$$e\phi_{n,ref} = k_BT\ln\left(\frac{N_0}{N_D} - 1\right). \quad (4)$$

This expression is similar to that for inorganic semiconductors with a free-electron-like conduction electron DOS, for which N_0 should be replaced by an effective mass and temperature-dependent effective value N_C [27].

Within the one-dimensional Schottky-contact model, the electrostatic potential due to the charged dopants and due to their image charges is taken to be laterally uniform. Whereas that may be a fair approximation for inorganic crystalline semiconductors, with delocalized

electron states, such an approximation is expected to be inappropriate for organic semiconductors with localized electron states. The effect of the Coulomb potential due to the positively charged dopants on the DOS is largest at the immediate nearest-neighbor molecules. At a distance a from a dopant molecule, the Coulomb energy is $E_{Coul,NN} = e^2/(4\pi\varepsilon_0\varepsilon_r a)$, so that in the limit of a small dopant concentration the DOS at these sites is given by

$$g_2(E) = \frac{1}{\sqrt{2\pi}\sigma}\exp\left(-((E + E_{Coul,NN})^2)/2\sigma^2)\right). \quad (5)$$

As a next refinement, we therefore consider the effect of a bimodal Gaussian DOS that is a superposition of the unperturbed DOS and the contribution due to host molecules at the nearest-neighbor (NN) positions around a dopant molecule. This model allows including integer charge-transfer complex (ICTC) formation, discussed in the Introduction. When each dopant is surrounded by Z nearest-neighbor molecules, the energy $e\phi_{n,dis+dop}$ for this approximate "disorder+dopants" model can be numerically determined using

$$N_D = \int_{-\infty}^{+\infty}\frac{g_1(E)\left[N_0 - (Z+1)N_D\right] + g_2(E)ZN_D}{1 + \exp\left((E + e\phi_{n,dis+dop})/k_BT\right)}dE. \quad (6)$$

This effective DOS approach, including only a NN-site correction, is similar to an effective DOS approach that has been suggested by Arkhipov *et al.* [8], albeit that we include in the total DOS the multiplicity of the NN sites and do not include in $g_2(E)$ an electric field dependence. We note that the Schottky-contact model already includes the Coulomb potential due to the dopants, albeit after lateral averaging of their positions, so that their effect is to a certain extent double counted. It is not obvious whether including the Coulomb potential at next-nearest-neighbor sites would improve the model or would worsen it due to more severe double counting. We therefore do not further refine the model to include such details. We show below that the disorder+dopants model provides a prediction of the depletion width that is for a wide range of material parameter values consistent with results of 3D-KMC simulations. Only for small depletion layer widths, when a dopant creates locally also a non-negligible image potential that partially screens the dopant potential, the model is found to somewhat overestimate the role of the dopants. In this work, we take $Z = 6$, as in a simple cubic lattice, and use $a = 1$ nm.

B. 3D-KMC simulations

The semianalytical models that have been presented do not yet include the full contribution to the DOS of the Coulomb potential resulting from the dopants and their

image charges. However, simply adding such contributions to the DOS would lead to a double-counting effect, as mentioned already in Sec. II A. Moreover, the Schottky-contact model neglects the small remaining electron charge density in the depletion zone and treats the transition to the charge-neutral region as abrupt. In order to be able to judge to what extent the various approximations that have been made are permitted, we use 3D-KMC simulations [28]. The simulations are carried out for monolayer electron-only devices such as shown in Fig. 1: an *n*-type uniformly doped organic layer is sandwiched in between two electrodes with the same work function. The thickness of the organic layer, L_x, is larger than $2W_D$ (typically $L_x = 100$ nm). Periodic boundary conditions are applied to the other two dimensions, with typical simulation box sizes $L_y = L_z = 50$ nm.

The molecules are taken to reside on the sites of a simple cubic lattice with an intermolecular distance $a = 1$ nm. Dopant molecules are assigned to randomly selected sites with a probability $N_D a^3$. We consider only materials with all ionized dopants, i.e., with a HOMO energy of the dopant molecules that is significantly higher than the LUMO energy of the host sites. The charge at each dopant site is therefore fixed, and equal to $+e$. The molecular site energies for the host molecules are randomly drawn from a Gaussian DOS with a width σ.

The 3D Coulomb potential around each individual charge carrier, resulting from all charge carriers and ionized dopants within a distance of $R_C = 10$ nm and including the image-charge effect near the metallic electrodes, is included in an exact manner [22]. The dielectric screening due to the thin-film environment is described by a distance-independent relative dielectric permittivity ε_r. The Coulomb interactions with charges at distances beyond R_C are treated using a layer-averaged one-dimensional (1D) Poisson equation. Double counting of short-range and long-range terms is avoided [22]. We verify that the results presented in this paper do not change when using a larger value of R_C. The site energies E_i thus include (i) the intrinsic Gaussian disorder energy, (ii) the short-range Coulomb interaction energy with the other charge carriers, the ionized dopants, and their image charges, (iii) the long-range layer-averaged Coulomb energy, and (iv) a correction to avoid double counting of the Coulomb interactions.

The electron hopping rate ω_{ij} from molecule i to j is described by the Miller-Abrahams formula [29]

$$\omega_{ij} = \nu_1 \exp\left[-\frac{2(R_{ij} - a)}{\lambda}\right] \exp\left(-\frac{|\Delta E_{ij}| + \Delta E_{ij}}{2k_B T}\right),$$
(7)

with R_{ij} the distance between the molecular sites i and j, ν_1 the NN hopping attempt rate, λ the wave-function decay length, and $\Delta E_{ij} = E_j - E_i$ the energy difference between

the sites i and j. The charge injection and collection rates are described by a Miller-Abrahams-type expression that is analogous to Eq. (7), with a spatial decay determined by the distance R_i from the molecular site i to the nearby electrode and with an energy change for injection and collection equal to $E_i - E_F$ and $E_F - E_i$, respectively, with E_F the Fermi energy of the electrode.

The depletion region thickness W_D in 3D-KMC simulations is extracted with caution. Firstly, the transition from depletion to charge neutrality is not abrupt; secondly, the intrinsic randomness in the LUMO energies and in the dopant positions leads to statistical variations of the layer-averaged electron density. Due to these reasons, we define W_D as the distance from the interface at which the charge-carrier density starts to be significantly lower than (in practice, typically 75%) the local dopant density. To minimize the uncertainty in W_D that results from this variation, we typically use averaged results of simulations for ten disorder configurations with otherwise the same set of parameters.

C. Results and discussion

Figure 2 shows a comparison of the depletion region widths that are obtained from the three semianalytical models that have been presented above and from 3D-KMC simulations. Table I lists the set of default material and device parameters for which the simulations have been performed. An injection barrier of 1 eV is assumed based on realistic material combinations [18,19]. The four panels in the figure show the sensitivity of W_D to a variation of one of the parameters. For the default set of parameters, the 3D-KMC simulations yield $W_D = 11.5$ nm. In the figure, this result is indicated by a red open square. Figure S1(a) within the Supplemental Material [30] shows for three different dopant concentrations how W_D is deduced from the electron concentration profile across the layer thickness. The error bars that are added to the 3D-KMC data points in Fig. 2 are based on the statistical variations in the layer-averaged concentrations.

The dependence of W_D on the dopant concentration is shown in Fig. 2(a). From the comparison with the KMC results, it is seen that the reference model (δ-function DOS and no dopant-induced energetically deep-lying states) significantly overestimates W_D, especially at low doping concentrations. The discrepancy becomes smaller when the effect of disorder is included. When also the effect of dopant-induced energetically deep-lying states is included, good agreement with the KMC results is obtained. The simulations show that for small dopant concentrations the shape of the Gaussian DOS is sensitively modified by the dopant-induced Coulomb interactions. However, near a dopant concentration of 10^{-2}, all models converge to almost the same value of W_D. The intrinsic Gaussian energetic disorder is at such high dopant concentrations
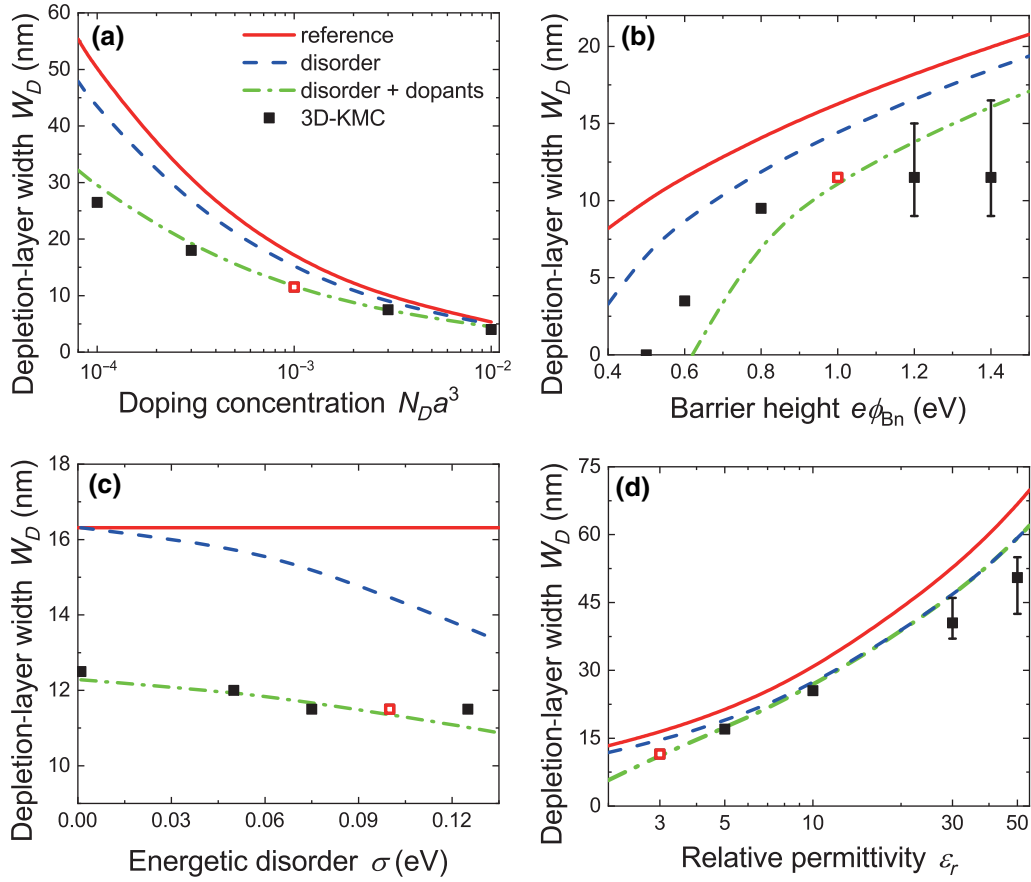
FIG. 2. Depletion layer width W_D in a Schottky contact formed by a metallic electrode and a doped disordered organic semiconductor at equilibrium ($V = 0$), as a function of (a) the dopant concentration $N_D a^3$, (b) the injection barrier height $e\phi_{Bn}$, (c) the energetic disorder energy σ, and (d) the relative dielectric constant ε_r. The parameters that are not varied are as given in Table I. The curves are results from the three semianalytical models of Sec. II A. The symbols are results from 3D-KMC simulations. The KMC result for the default parameter set is indicated by a red open square in (a)–(d).

overridden by the Coulomb interactions, and the ensemble of interacting electrons and dopant charges behaves in a manner more similar to that in a conventional inorganic semiconductor device.

Figure 2(b) shows the dependence of W_D on the injection barrier height $e\phi_{Bn}$. W_D approaches zero around $e\phi_{Bn} \approx 0.5$ eV. Across the entire range of barrier heights that is considered, W_D is found to be smaller than the

TABLE I. Overview of default material and device parameters.

Parameter	Value
Layer thickness L_x	100 nm
Energetic disorder width σ	0.1 eV
Hopping attempt frequency ν_1	3.3×10^{10} s^{-1}
Wave-function decay length λ	0.3 nm
Relative dielectric permittivity ε_r	3
Temperature T	290 K
Dopant concentration $N_D a^3$	10^{-3}
Injection barrier height $e\phi_{Bn}$	1 eV

values that are obtained without including the effect of dopant-induced energetically deep-lying states. For small barriers, including that effect by using the disorder+dopants model [Eq. (6)] is seen to slightly overestimate the effect of the dopant-induced potential. We attribute this overestimation to the image-charge screening of that effect, which becomes more relevant for small values of W_D. For large barrier heights (above approximately 1 eV), the 3D-KMC simulations do not reach a thermal equilibrium state within a reasonable simulation time, as discussed in more detail in Sec. IV. This leads to the indicated large error bars. A proper comparison with the semianalytical results can then not be made.

Figure 2(c) shows that the semianalytical disorder+dopants model provides a fair description of the (weak) dependence of W_D on the disorder energy σ, and Fig. 2(d) shows that that model also provides a fair description of the dependence on the relative permittivity. When no dopant-induced energy-level shifts are included, W_D varies as $\sqrt{\varepsilon_r}$ [see Eq. (1)]. The ε_r^{-1} dependence of the dopant-induced energy shifts leads to a slightly deviating

ε_r dependence, in particular in the low-ε_r range. We note that in all simulations L_x is taken larger than $2W_D$, up to 150 nm, to avoid any interaction between the two depletion zones.

Whereas a weak temperature dependence of W_D would be expected from all three semianalytical models, including the disorder+dopants model, the 3D-KMC simulations do not show such an effect (Fig. S2 within the Supplemental Material [30]). We attribute that to some thermally induced dissociation of bound electron-dopant pairs at the charge-neutral layer side of the depletion layer boundary. The resulting increase of W_D then compensates the decrease of W_D due to thermal excitation of electrons from the electrode to low-energy states in the semiconductor in the depletion region near the transition to the charge-neutral region. The overall effect is then just a decrease of the abruptness of the transition with increasing temperature, but not a change of W_D.

III. CHARGE-CARRIER MOBILITY

In the previous section, we find that under equilibrium conditions the width of the depletion region is well predicted using the semianalytical disorder+dopants model [Eq. (6)] and that for the cases studied the use of this refined model is useful for dopant concentrations below 10^{-2}. Under nonequilibrium conditions, at finite voltages, the steady state and transient device performance depends on the voltage drops across the two depletion zones and across the charge-neutral bulk layer. In order to be able to extend the semianalytical models that are developed in Sec. II to nonequilibrium conditions (in Secs. IV and V), and in order to obtain deeper insight into the effects of the dopants on the electron transport, we study in this section the electron mobility in charge-neutral and non-neutral materials.

A. Electron mobility in the charge-neutral state

We calculate the electric field dependence of the electron mobility in charge-neutral uniformly *n*-doped disordered organic semiconductors using 3D-KMC simulations at various doping concentration and for disorder energies of 0.05 and 0.10 eV. The simulations are carried out for $100 \times 100 \times 100$ nm boxes with periodic boundary conditions. Otherwise, the approach is identical to that described in Sec. II B and in Refs. [17,24]. The simulation results complement earlier systematic studies of the charge-carrier concentration and temperature dependence of mobility in molecularly doped systems [9–13]. Results of studies of the electric field dependence have not yet been reported.

Figure 3 gives an overview of the results. All data shown are well described using a function $\mu(F) = \mu_0 \exp[(F/F_0)^{0.434}]$ with two fit parameters: the mobility in the limit of zero field, μ_0, and a characteristic electric field F_0. Their values are included in Table II.
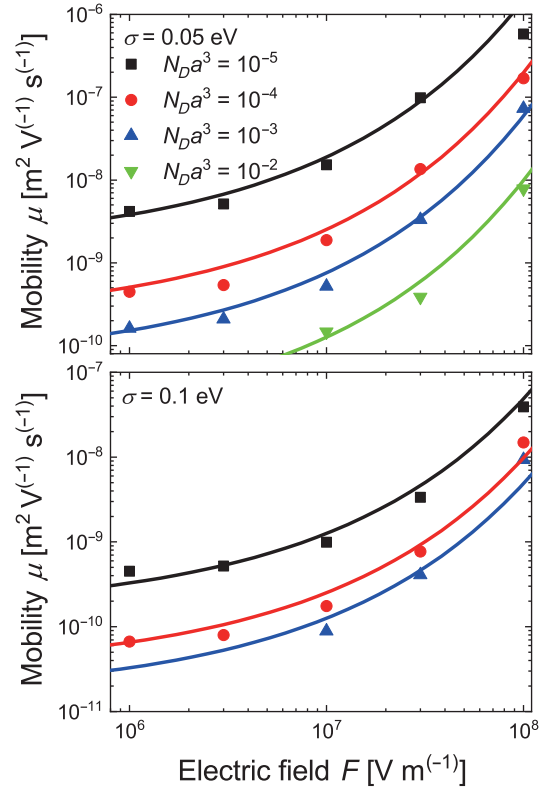

FIG. 3. Electric field F dependence of the charge-carrier mobility μ of charge-neutral doped disordered organic semiconductors, at various doping concentrations $N_D a^3$ and energetic disorders σ. The symbols are results of 3D-KMC simulations. The results of curves are parametrized fitting functions $\mu = \mu_0 \exp[(F/F_0)^{0.434}]$, with values of μ_0 and F_0 given in Table II.

It is interesting that μ_0 depends on the doping concentration as well as on and the energetic disorder, while F_0 depends only on the energetic disorder. Consistent with reported experimental results for low and moderate energetic disorder cases [11,31], the mobility is found to decrease with increasing dopant concentration, resulting in

TABLE II. Values of the parameters determining the electric field dependence of the electron mobility of charge-neutral disordered organic semiconductors with *n*-type molecular dopants that are all ionized.

Doping concentration $N_D a^3$	Disorder energy σ (eV)	μ_0 [m^2 V$^{(-1)}$ s$^{(-1)}$]	F_0 [10^6 V m$^{(-1)}$]
10^{-5}	0.05	1.5×10^{-9}	1.17
10^{-4}	0.05	2.0×10^{-10}	1.17
10^{-3}	0.05	6.0×10^{-11}	1.17
10^{-2}	0.05	1.0×10^{-11}	1.17
10^{-5}	0.1	1.5×10^{-10}	1.76
10^{-4}	0.1	3.0×10^{-11}	1.76
10^{-3}	0.1	1.5×10^{-11}	1.76

a sublinear dopant concentration dependence the electrical conductivity.

B. Electron mobility in non-neutral materials

The findings of a strong decrease of the mobility in charge-neutral materials with increasing dopant concentration, in the previous subsection, and of an ultraslow formation of the depletion zone, discussed briefly in Sec. III.C and more extensively in Sec. V, can be understood by studying the electron mobility in non-charge-neutral systems. We perform such studies using 3D-KMC simulations, following the same methodology as used above for the case of charge-neutral systems. Figure 4 gives an overview of the carrier-concentration (c) dependence of the mobility that has been obtained for various values of the dopant concentration $N_D a^3$ and the electric field, for a disorder energy of 0.05 eV. When $c = N_D a^3$, the system is charge neutral. The mobility is then equal to the corresponding value in Fig. 3.

The figure shows for small dopant concentrations [panels (a) and (b)] a clear transition from a small concentration regime ($c < N_D a^3$, realistically for moderate and high injection barrier cases) to a large concentration regime ($c > N_D a^3$, realistically for very low injection

barrier cases). When $c < N_D a^3$, the mobility is reduced dramatically due to strong binding of the electrons with the positively charged dopants, leading to the formation of integer charge transfer complexes (ICTCs). When $c > N_D a^3$, the excess electrons are not paired to immobile ionized dopants and are free to move, thus leading to a high mobility. Such a transition from trap-dominated to trap-filled transport is a well-known phenomenon in the transport physics of inorganic and organic semiconductors [32,33]. At a high external electric field, the external field dominates over the intrinsic mutual attraction between a charge carrier and an ionized dopant. The ICTCs are then pulled apart and most of the charge carriers become free to move. In the limit of small c the mobility becomes carrier-concentration independent because the transport is then in the independent-particle (Boltzmann) regime [34].

For intermediate dopant concentrations [panel (c)] a transition to an alternative regime becomes visible, in which the electron-electron and electron-dopant Coulomb interactions reduce the mobility for positively and negatively charged systems. The mobility decreases at high charge-carrier concentrations because the charge-carrier transport is impeded by the enhanced energetic disorder due to nearby charge carriers and ionized dopants [24]. For the very high doping concentration case $N_D a^3 = 10^{-2}$
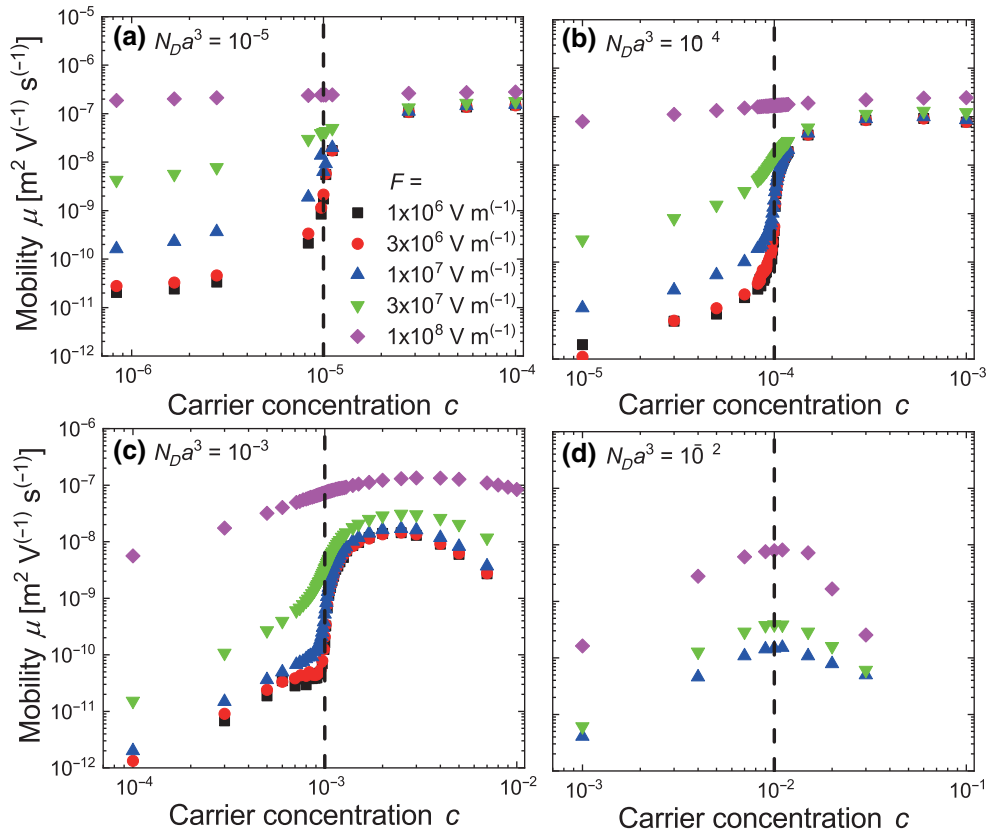

FIG. 4. Calculated charge-carrier mobility μ as a function of the charge-carrier concentration c at various doping concentrations $N_D a^3$ and electric fields F, calculated using 3D-KMC simulations for systems with a disorder energy of $\sigma = 0.05$ eV.

in panel (d), the system becomes similar to a "Coulomb glass." The reduction of the mobility by the Coulomb correlations of the entire ensemble of charges (instead of the individually paired ICTCs) dominates over the increased mobility by the unpaired excess electrons. We comment here that at such a high doping concentration the incoherent hopping and localized charge-carrier model used throughout this work may need further refinement, as studies of the doping dependence of the conductivity of conjugated polymers, e.g., have provided evidence of a growing delocalization with increasing state filling [35]. For systems with a larger energetic disorder ($\sigma = 0.1$ eV), similar trends in the mobility are obtained (see Fig. S3 within the Supplemental Material [30]), albeit that the steepness of the increase of the mobility with increasing c around the charge-neutrality concentration is significantly reduced.

IV. DEPLETION REGION WIDTH—FINITE BIAS VOLTAGE

In this section we show how the semianalytical models that have been presented in Sec. II A can be extended to finite-bias-voltage conditions. We use the description of the charge-carrier density and electric field dependence of the mobility of electrons in uniform charge-neutral and charged molecularly doped layers that has been presented in the previous section and give for double Schottky barrier devices a comparison between the extended semianalytical model and 3D-KMC simulation results. The comparison focusses on the different depletion layer widths near the left and right electrodes and on the total current density.

A. Semianalytical models

We study single-layer double Schottky barrier devices such as shown in Fig. 5(a), based on a disordered molecularly doped *n*-type organic semiconductor. The Schottky contact formed with the left (right) electrode is forward (reverse) biased. As indicated in the figure, the partial voltages over the left and right Schottky barriers are called V_F and V_R, respectively, and the voltage drop across the bulk of the doped semiconductor is called V_B. These voltages induce current densities J_F, J_R, and J_B, respectively, in these three parts of the device, which should be equal.

For disordered organic semiconductors, three modifications need to be applied to the general form of the conventional double Schottky device models, used for inorganic crystalline semiconductors [27,36]: (i) due to the low charge-carrier mobility, the voltage drop V_B across the bulk of the doped semiconductor cannot be neglected, (ii) due to the hopping transport mechanism, the charge-injection process is diffusion limited rather than thermionic emission dominated [27], and (iii) the charge-carrier densities $n(0) = n(L_x)$ at the metal interfaces depend on the width of the Gaussian DOS, and are given by the right-hand side of Eq. (3) after replacing $e\phi_n$ by $e\phi_{Bn}$. The
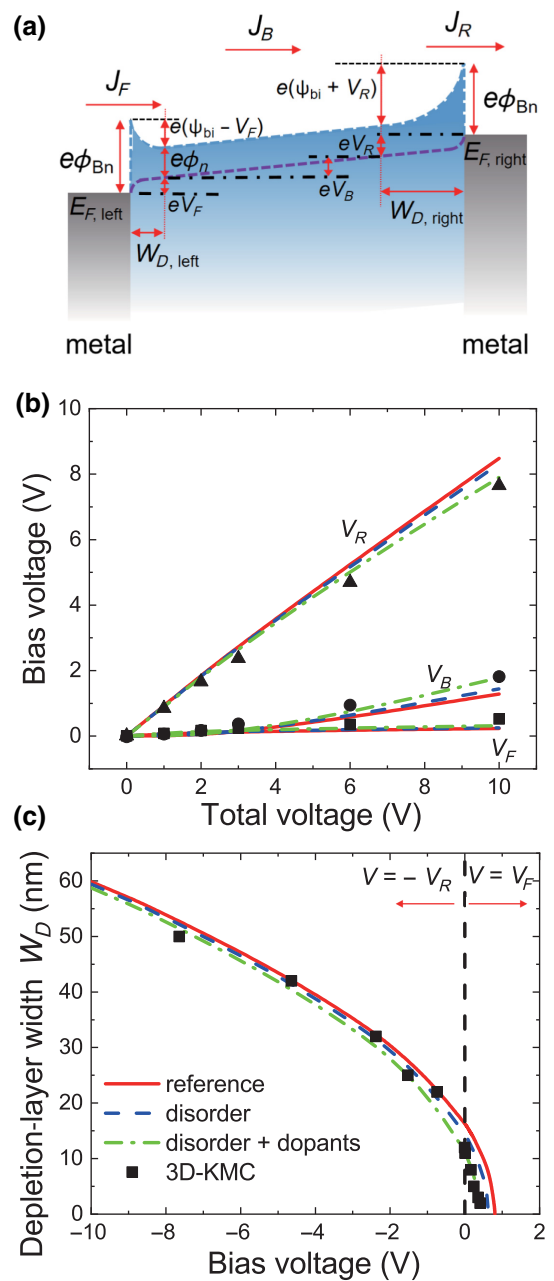

FIG. 5. (a) Energy diagram of the same device as in Fig. 1, at $V > 0$. V_F, V_R, and V_B are the voltage drops across the left and right Schottky junctions, and the bulk of the semiconductor. (b) V_F, V_R, and V_B as a function of the total applied voltage V, calculated from semianalytical models using Eq. (8) (curves) and 3D-KMC simulations (symbols). (c) Depletion layer width W_D as a function of the bias voltage across both Schottky junctions, calculated from semianalytical models (curves) and 3D-KMC simulations (symbols).

partial voltages follow by solving under the constraints $V_F + V_B + V_R = V$ and $J_F = J_R = J_B$ (current continuity) the following set of equations for the current densities in each part of the device [27]:

$$J_F = \frac{e^2 D_n n(0)}{k_B T} \sqrt{\frac{2 e N_D (\psi_{\text{bi}} - V_F)}{\varepsilon_0 \varepsilon_r}} \exp\left[\frac{e}{k_B T}\left(\frac{e^3 N_D (\psi_{\text{bi}} - V_F)}{8\pi^2 \varepsilon_0^3 \varepsilon_r^3}\right)^{1/4}\right]\left[\exp\left(\frac{e V_F}{k_B T}\right) - 1\right], \tag{8a}$$

$$J_R = \frac{e^2 D_n n(L_x)}{k_B T} \sqrt{\frac{2 e N_D (\psi_{\text{bi}} + V_R)}{\varepsilon_0 \varepsilon_r}} \exp\left[\frac{e}{k_B T}\left(\frac{e^3 N_D (\psi_{\text{bi}} + V_R)}{8\pi^2 \varepsilon_0^3 \varepsilon_r^3}\right)^{1/4}\right]\left[1 - \exp\left(-\frac{e V_R}{k_B T}\right)\right], \tag{8b}$$

$$J_B \approx N_D e \mu_n (F_B) F_B, \quad \text{with } F_B \approx \frac{V - V_F - V_R}{L_x - \sqrt{(2\varepsilon_0 \varepsilon_r / e N_D)\left(\psi_{\text{bi}} - V_F - (k_B T / e)\right)} - \sqrt{(2\varepsilon_0 \varepsilon_r / e N_D)\left(\psi_{\text{bi}} + V_R - (k_B T / e)\right)}}. \tag{8c}$$

Here D_n is the electron diffusivity that is obtained from the generalized Einstein equation $D_n = (\mu_n / e)(n(0, L_x) / dn(0, L_x)/d(e\phi_n))$, and $\mu_n(F)$ is the electric-field-dependent electron mobility. In the expressions for J_F and J_R the first exponential factor describes the image-potential-induced injection barrier lowering effect [27]. In the bulk of the device, charge neutrality is maintained. Therefore, the electric field F_B in this region is constant and simply equal to the ratio of the voltage drop and the bulk region thickness. As a result of the doping uniformity, the electron density gradient is in the bulk region insignificant, so that the current density does not contain a diffusion term. The electron mobility in the bulk region depends strongly on the local electric field. The simulated mobility is parameterized using a fitting function obtained in Sec. III A. The values of $\phi_n(N_D)$ that determine ψ_{bi} in Eq. (8) [using $\psi_{\text{bi}} = \psi_{Bn} - \phi_n(N_D)$] do not depend on V. However, they are different for each of the three semianalytical models that have been presented in Sec. II A, and follow from Eqs. (3), (4), and (6).

B. Results and discussion

Figure 5(b) shows a comparison of the partial voltages V_F, V_R, and V_B that have been obtained from the various semianalytical models and from 3D-KMC simulations for the set of material and device parameters that is given in Table I. The 3D-KMC simulations are carried out as described in Sec. II B. The site energies now include a contribution due to the applied field that varies linearly with position x [22]. The current densities that for each voltage V are obtained from the full-device 3D-KMC simulations are used to derive from Eq. (8) the voltage drops V_F, V_R, and V_B and to derive subsequently using Eq. (1) the depletion regions width W_D for each junction. This is done as follows. For a given voltage and current density, Eq. (8c) provides a first (implicit) relation between V_F and V_R. Furthermore, by equating the right-hand-sides of Eqs. (8a) and (8b) a second implicit relation between V_F and V_R is obtained. All other quantities that enter the expression for J_B are known. By solving this set of two equations, both voltages are obtained. We note that this approach assumes

that the diffusivity $D_n \approx D_n(0, L_x)$ is constant and thus cancels out, albeit that in principle D_n depends on the carrier concentration and the electric field, which varies spatially within the depletion layer. Nevertheless, Fig. 5(b) shows that the semianalytical model provides values of all three partial voltages that are in fair agreement with the 3D-KMC simulation results, in particular the disorder+dopants model (green dashed-dotted curves). The analysis shows that most of the applied voltage drops over the reverse-biased Schottky junction and that at large voltages V_B becomes significantly higher than V_F.

In Fig. 5(c) the calculated depletion layer widths are compared. The width of the forward-biased depletion region, $W_{D,\text{left}}$ is very small. The disorder+dopants model agrees then significantly better with the 3D-KMC results than the reference model, which neglects energetic disorder and the dopant-induced modification of the DOS. The predicted width of the reverse-biased depletion region, $W_{D,\text{right}}$, becomes already at relatively low voltages (≤ -1 V), quite insensitive to the modeling details. That may be understood from Eq. (1): the voltage drop V_R across that junction becomes then for each model much larger than ψ_{bi}. We conclude that also for finite voltages the semianalytical disorder+dopants model provides a good description of the depletion-region widths.

V. SCHOTTKY-CONTACT FORMATION DYNAMICS

In conventional inorganic semiconductors devices, the delocalized nature of the charge carrying states and the associated high mobility leads to ultrafast (femtosecond scale) formation dynamics of Schottky junctions. The much lower charge-carrier mobility in disordered organic semiconductors is expected to lead to much slower dynamics. A first indication of ultraslow depletion-region formation is already reported in Sec. II C, where for systems with large electron injection barriers ($e\phi_{Bn} = 1.2$ and 1.4 eV) the 3D-KMC simulation results (mean values) are found to deviate from all semianalytical model predictions.

We study the dynamics of Schottky-junction formation by carrying out 3D-KMC simulations for devices such as

shown in Fig. 5(a), starting at time $t = 0$ with either an entirely charge-neutral device or a fully depleted device. The simulations are carried out using the parameters given in Table I. Figure 6 shows the evolution of the normalized total number of electrons in the devices for various applied voltages and for two injection barrier heights. The calculated system equilibration time is seen to vary greatly, from microseconds to beyond tens of milliseconds. In most cases, an applied voltage or a lower injection barrier can significantly accelerate the transient charge-carrier dynamics. For the $e\phi_{Bn} = 1.2$ eV case with the fully depleted initial configuration, the $V = 1$ and 3 V cases show an even slower transient than the $V = 0$ V case. This may be understood from the fact that at $V = 0$ V charge injection can occur at both sides of the device, whereas at $V = 1$ or 3 V the forward-biased injection is not significantly enhanced

while the reversed biased is further suppressed. We note that the accuracy of all 3D-KMC results in Figs. 2 and 5 is carefully checked by comparing results that are obtained for the two initial conditions. All results are well converged to the steady state, except for the high-injection-barrier cases ($e\phi_{Bn} = 1.2$ and 1.4 eV). In order to experimentally validate the slow dynamics of Schottky-junction formation, possible methods might be to use the device structure in Fig. 5(a) and probe the transient current density in the presence of an abrupt voltage change or measure the capacitance-voltage characteristics.

VI. SUMMARY AND OUTLOOK

We systematically investigate the formation of Schottky contacts formed between a metallic electrode and a molecularly doped disordered organic semiconductor. Using 3D-KMC simulations, we find that the depletion-layer width W_D is lower than as expected for conventional inorganic semiconductors. The effect can be modeled well by an adapted form of the conventionally used expression for W_D [Eq. (1)], containing a dopant-density-dependent Fermi energy in the bulk of the semiconductor (ϕ_n for n-doped materials) that includes the effects of charge-carrier localization, energetic disorder, and the integer charge-transfer complex (ICTC) formed by an ionized dopant and a released charge carrier [Eq. (6)]. In the first part of the paper, this is demonstrated for contacts under equilibrium conditions. In the second part, the effect of a bias voltage on the current density in metal-semiconductor-metal devices is studied. For such double-Schottky devices, a modified form of the conventionally used expressions for the current density [Eq. (8)] is found to provide a good description of the $J(V)$ characteristics. The model includes the adapted form of the bulk value of ϕ_n, a description of injection as a diffusion-limited process and the finite voltage drop across the bulk part of the device. In the third part of the paper, we demonstrate from 3D-KMC simulations that the low charge-carrier mobility in disordered organic semiconductors leads to much slower dynamics of the Schottky-contact formation process, depending on the injection barrier, than in conventional crystalline inorganic semiconductor devices.

We assume in this paper that the dopants are all ionized. It would be interesting to study in future work systems in which not all dopants are ionized, i.e., n-doped materials in which the HOMO of the dopant molecule is close to or lower than the LUMO of the host molecule [10]. It would also be interesting to explore the Schottky-contact formation process for host materials with an exponential DOS, such as often observed from studies of electron transport [9], in addition to host materials with a Gaussian DOS studied in this work. Another interesting next step is to combine 3D-KMC models with molecular-level
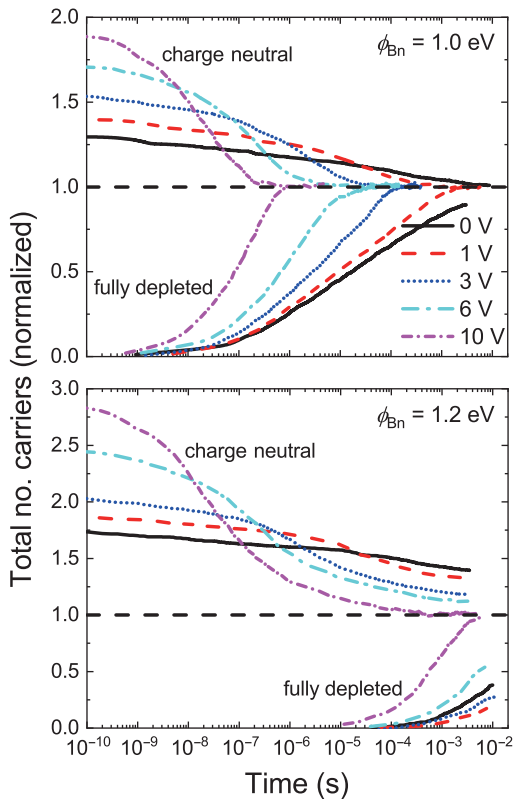

FIG. 6. Evolution of the total number of charge carriers in a device such as shown in Fig. 5(a), as a function of time for various applied voltages at two injection barrier heights $\phi_{Bn} = 1$ eV (a) and 1.2 eV (b), calculated from 3D-KMC simulations. The numbers of charge carriers are normalized with respect to their steady-state values. The simulation parameters are as given in Table I. The upper part in each panel gives the simulation results that are obtained after starting with a charge-neutral configuration. The charge carriers flow then out to the electrodes so that the two depletion layers are formed. The lower parts give the simulation results that are obtained after starting with a fully depleted configuration. Charge carriers are then injected from the electrodes and fill the bulk of the device.

first-principles calculations for dopant-host combinations [5,10,11].

---

[1] B. Geffroy, P. le Roy, and C. Prat, Organic light-emitting diode (OLED) technology: materials, devices and display technologies, Polym. Int. **55,** 572 (2006).

[2] I. Salzmann, G. Heimel, M. Oehzelt, S. Winkler, and N. Koch, Molecular electrical doping of organic semiconductors: Fundamental mechanisms and emerging dopant design rules, Acc. Chem. Res. **49,** 370 (2016).

[3] J. Kido and T. Matsumoto, Bright organic electroluminescent devices having a metal-doped electron-injecting layer, Appl. Phys. Lett. **73,** 2866 (1998).

[4] X. Zhou, M. Pfeiffer, J. Blochwitz, A. Werner, A. Nollau, T. Fritz, and K. Leo, Very-low-operating-voltage organic light-emitting diodes using a p-doped amorphous hole injection layer, Appl. Phys. Lett. **78,** 410 (2001).

[5] M. Schwarze, C. Gaul, R. Scholz, F. Bussolotti, A. Hofacker, K. S. Schellhammer, B. Nell, B. D. Naab, Z. Bao, and D. Spoltore, *et al.*, Molecular parameters responsible for thermally activated transport in doped organic semiconductors, Nat. Mater. **18,** 242 (2019).

[6] X. Zhou, J. Blochwitz, M. Pfeiffer, A. Nollau, T. Fritz, and K. Leo, Enhanced hole injection into amorphous hole-transport layers of organic light-emitting diodes using controlled p-type doping, Adv. Funct. Mater. **11,** 310 (2001).

[7] R. Warren, A. Privitera, P. Kaienburg, A. E. Lauritzen, O. Thimm, J. Nelson, and M. K. Riede, Controlling energy levels and Fermi level en route to fully tailored energetics in organic semiconductors, Nat. Commun. **10,** 1 (2019).

[8] V. I. Arkhipov, P. Heremans, E. V. Emelianova, and H. Bässler, Effect of doping on the density-of-states distribution and carrier hopping in disordered organic semiconductors, Phys. Rev. B **71,** 045214 (2005).

[9] M. L. Tietze, J. Benduhn, P. Pahner, B. Nell, M. Schwarze, H. Kleemann, M. Krammer, K. Zojer, K. Vandewal, and K. Leo, Elementary steps in electrical doping of organic semiconductors, Nat. Commun. **9,** 1 (2018).

[10] A. Fediai, A. Emering, F. Symalla, and W. Wenzel, Disorder-driven doping activation in organic semiconductors, Phys. Chem. Chem. Phys. **22,** 10256 (2020).

[11] A. Fediai, F. Symalla, P. Friederich, and W. Wenzel, Disorder compensation controls doping efficiency in organic semiconductors, Nat. Commun. **10,** 1 (2019).

[12] G. Zuo, H. Abdalla, and M. Kemerink, Impact of doping on the density of states and the mobility in organic semiconductors, Phys. Rev. B **93,** 235203 (2016).

[13] M. Koopmans, M. A. T. Leiviskä, J. Liu, J. Dong, L. Qiu, J. C. Hummelen, G. Portale, M. C. Heiber, and L. J. A. Koster, Electrical conductivity of doped organic semiconductors limited by carrier–carrier interactions, ACS. Appl. Mater. Interfaces **12,** 56222 (2020).

[14] A. D. Özdemir, S. Kaiser, T. Neumann, F. Symalla, and W. Wenzel, Systematic kMC study of doped hole injection layers in organic electronics, Front. Chem. **9,** 809415 (2022).

[15] C. Tanase, E. J. Meijer, P. W. M. Blom, and D. M. de Leeuw, Unification of the Hole Transport in Polymeric Field-Effect Transistors and Light-Emitting Diodes, Phys. Rev. Lett. **91,** 216601 (2003).

[16] C. Tanase, P. W. M. Blom, and D. M. de Leeuw, Origin of the enhanced space-charge-limited current in poly(p-phenylene vinylene), Phys. Rev. B **70,** 193202 (2004).

[17] W. F. Pasveer, J. Cottaar, C. Tanase, R. Coehoorn, P. A. Bobbert, P. W. M. Blom, D. M. de Leeuw, and M. A. J. Michels, Unified Description of Charge-Carrier Mobilities in Disordered Semiconducting Polymers, Phys. Rev. Lett. **94,** 206601 (2005).

[18] B. Lüssem, M. Riede, and K. Leo, Doping of organic semiconductors, Phys. Status Solidi (a) **210,** 9 (2013).

[19] M. Pfeiffer, K. Leo, X. Zhou, J. Huang, M. Hofmann, A. Werner, and J. Blochwitz-Nimoth, Doped organic semiconductors: Physics and application in light emitting diodes, Org. Electron. **4,** 89 (2003).

[20] B. Yurash, D. X. Cao, V. V. Brus, D. Leifert, M. Wang, A. Dixon, M. Seifrid, A. E. Mansour, D. Lungwitz, and T. Liu, *et al.*, Towards understanding the doping mechanism of organic semiconductors by Lewis acids, Nat. Mater. **18,** 1327 (2019).

[21] H. Bässler, Charge transport in disordered organic photoconductors a Monte Carlo simulation study, Phys. Status Solidi (b) **175,** 15 (1993).

[22] J. J. M. van der Holst, F. W. A. van Oost, R. Coehoorn, and P. A. Bobbert, Monte Carlo study of charge transport in organic sandwich-type single-carrier devices: Effects of Coulomb interactions, Phys. Rev. B **83,** 085206 (2011).

[23] M. Mesta, M. Carvelli, R. J. de Vries, H. van Eersel, J. J. van der Holst, M. Schober, M. Furno, B. Lüssem, K. Leo, and P. Loebl, *et al.*, Molecular-scale simulation of electroluminescence in a multilayer white organic light-emitting diode, Nat. Mater. **12,** 652 (2013).

[24] F. Liu, H. van Eersel, B. Xu, J. G. E. Wilbers, M. P. de Jong, W. G. van der Wiel, P. A. Bobbert, and R. Coehoorn, Effect of Coulomb correlation on charge transport in disordered organic semiconductors, Phys. Rev. B **96,** 205203 (2017).

[25] F. Liu, Y. Su, X. Lin, L. Nian, B. Wu, Q. Niu, H. van Eersel, P. A. Bobbert, R. Coehoorn, and G. Zhou,

Image-Force-Stabilized Interfacial Dipole Layer Impedes Charge Injection into Disordered Organic Semiconductors, Phys. Rev. Appl. **17**, 024003 (2022).

[26] S. Gottardi, M. Barbry, R. Coehoorn, and H. van Eersel, Efficiency loss processes in hyperfluorescent OLEDs: A kinetic Monte Carlo study, Appl. Phys. Lett. **114**, 073301 (2019).

[27] S. M. Sze, Y. Li, and K. K. Ng, *Physics of Semiconductor Devices* (Wiley, Hoboken, New Jersey, 2021).

[28] The 3D-KMC tool used in this work is Bumblebee, provided by Simbeyond B.V. (simbeyond.com).

[29] A. Miller and E. Abrahams, Impurity conduction at low concentrations, Phys. Rev. **120**, 745 (1960).

[30] See the Supplemental Material at http://link.aps.org/supplemental/10.1103/PhysRevApplied.19.024041 for additional simulation results of charge-carrier profile, temperature dependence of the depletion region width, and charge-carrier mobility for non-charge-neutral doped disordered organic semiconductors.

[31] P. Pingel and D. Neher, Comprehensive picture of p-type doping of P3HT with the molecular acceptor F_4 TCNQ, Phys. Rev. B **87**, 115209 (2013).

[32] M. A. Lampert and P. Mark, *Current Injection in Solids* (Academic Press, New York, 1981).

[33] K. C. Kao and W. Hwang, *Electrical Transport in Solids* (Pergamon, Oxford, New York, 1981).

[34] R. Coehoorn, W. F. Pasveer, P. A. Bobbert, and M. A. J. Michels, Charge-carrier concentration dependence of the hopping mobility in organic materials with Gaussian disorder, Phys. Rev. B **72**, 155206 (2005).

[35] H. C. F. Martens, I. N. Hulea, I. Romijn, H. B. Brom, W. F. Pasveer, and M. A. J. Michels, Understanding the doping dependence of the conductivity of conjugated polymers: Dominant role of the increasing density of states and growing delocalization, Phys. Rev. B **67**, 121203 (2003).

[36] A. Grillo and A. Di Bartolomeo, A current-voltage model for double Schottky barrier devices, Adv. Electron. Mater. **7**, 2000979 (2021).